ELSEVIER

Materials Science and Engineering A 413–414 (2005) 192–199

MATERIALS SCIENCE & ENGINEERING A

www.elsevier.com/locate/msea

Study of spatial phase separation during solidification and its impact on the formation of macrosegregations

Menghuai Wu*, Andreas Ludwig

Simulation and Modeling of Metallurgical Processes, Christian–Doppler-Lab for Multiphase Modeling of Metallurgical Processes, Department of Metallurgy, University of Leoben, Franz-Josef-Street 18, A-8700 Leoben, Austria

Received in revised form 11 July 2005

Abstract

With the term "spatial phase separation" we have the relative motion between two or more liquid and/or solid phases in mind. This relative motion can be caused by thermo-solutal melt convection, grain sedimentation, sedimentation-induced melt convection, feeding flow through stationary (columnar) or packed (equiaxed) grains, and capillary force driven melt flow (Marangoni). A multiphase solidification model considering the above mentioned phase separation phenomena has been developed by the authors. This paper provides selected modeling results in order to demonstrate the importance of phase separation for the formation of macrosegregations and hence to deepen our understanding of different macrosegregation formation mechanisms.

Keywords: Multiphase modeling; Solidification; Macrosegregation; Spatial phase separation; Melt convection; Grain sedimentation

1. Introduction

Since the pioneering works by Flemings and co-workers in the 1960s [1–4], the understanding of the formation of macrosegregation has been significantly improved. It became clear that convection within the mushy zone, the interdendritic flow is directly related to the formation of macrosegregations (Fig. 1). With this knowledge, over years numerous improvements of industrial processes were gained. However, most of the pioneering works were done analytically, and limited to 1D or simplified 2D cases. Real modeling efforts on understanding the formation of macrosegregations were made only very recently [5]. Nowadays with the increasing computation power and the advanced CFD software, the solidification process is modeled by including the forced or natural (thermal–solutal) convection, interdendritic feeding flow, and even the deformation-induced flow by advanced multiphase modeling.

The authors have developed a two phase solidification model based on an Eulerian approach [6–11]. The flow phenomena mentioned above (except the deformation-induced flow) were taken into account. This model was recently extended to a more general case, i.e. the mixed columnar and equiaxed solidification [12]. The model accounts for the different origins for macrosegregation formation, as summarized by Beckermann [5]. However, in the present paper we do not invoke the applied model considerations in details as they can be found in [6–12]. This paper provides three selected modeling results which demonstrate the importance of the relative motion of different liquid and/or solid phases for the formation of macrosegregations.

2. The numerical model and calculation of the mixture concentration c_{mix}

In the Eulerian approach, the phases which appear during solidification are considered as interpenetrating continua. In a two-phase solidification model, only liquid (l) and solid (s), are considered, while in the mixed columnar and equiaxed solidification model, three phases are considered, i.e. liquid (l), equiaxed (e) and columnar (c). Although the thermodynamic properties of the equiaxed and columnar phases are same, their hydrodynamic behaviors are different. Conservation equations of mass, momentum, energy, and species for each phase are solved except the momentum conservation equation for the columnar phase. Closure laws for each conservation equations are defined by taking into account the solidification

* Corresponding author. Tel.: +43 3842 4022223; fax: +43 3842 4022202.
E-mail address: menghuai.wu@notes.unileoben.ac.at (M. Wu).

0921-5093/$ – see front matter © 2005 Elsevier B.V. All rights reserved.
doi:10.1016/j.msea.2005.09.051

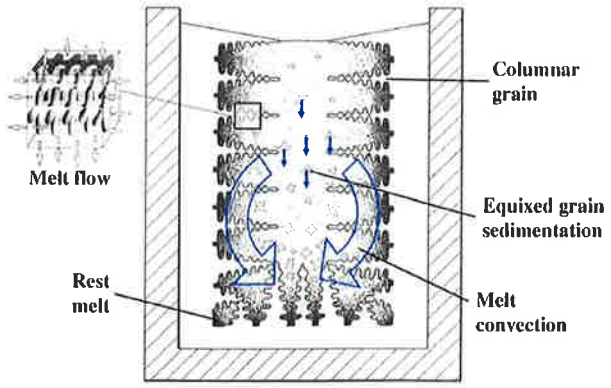

Fig. 1. Schematic illustration of solidification and flow phenomena in a simplified ingot [1].

thermodynamics, grain growth kinetics, interfacial hydrodynamical interactions, release of latent heat and interphasic heat and species exchanges at the solidifying solid–liquid interface. Details about the numerical model are described in original publications [6–12]. As modeling results we obtain the volume averaged quantities such as temperature T_q, volume fraction of phases f_q, velocity $\vec{u}_q$, and species concentration c_q^i. Here the subscript q is the phase index and the superscript i the species index which is used for multicomponent systems only. In order to quantify the macrosegregation in multiphase systems, a mixture concentration c_{mix} is defined as

$$c_{mix} = \frac{\sum_{q=1}^{n} c_q f_q \rho_q}{\sum_{q=1}^{n} f_q \rho_q} \quad (1)$$

3. Case studies

3.1. Case I: macrosegregation due to interdendritic flow

In order to address the formation of macrosegregation due to interdendritic flow, this case considers only columnar solidification. Nucleation of equiaxed grains is intentionally 'suppressed'. As solidification shrinkage is also ignored, the interdendritic flow is caused only by the thermal–solutal convection. A Boussinesq approximation is used, so that for all conservation equations both liquid and solid are considered to have the same density, $\rho_s = \rho_l$, except in the momentum conservation equation where a corresponding thermal–solutal buoyancy force is applied as a source term $\vec{F}_{T-S}$:

$$\vec{F}_{T-S} = f_l \rho_l \vec{g} = f_l \rho_l^{ref} [\beta_T (T^{ref} - T_l) + \beta_c (c_l^{ref} - c_l)] \vec{g} \quad (2)$$

Here $\vec{g}$ is gravity acceleration, ρ_l^{ref} the reference density at the reference temperature T^{ref} and reference concentration c_l^{ref} and β_T and β_c are the thermal and solutal expansion coefficients.

The solidification of a binary "steel" (Fe–0.34 wt.% C) ingot casting with a relatively small size (diameter: 66 mm, height: 170 mm) is simulated (see Fig. 2). The casting is filled instantaneously, so we consider the start of solidification from a uniform initial temperature of 1785 K. The considered expansion coefficients are $\beta_T = 2 \times 10^{-4}$ (K^{-1}) and $\beta_c = 1.1 \times 10^{-2}$ ($wt.\%^{-1}$).

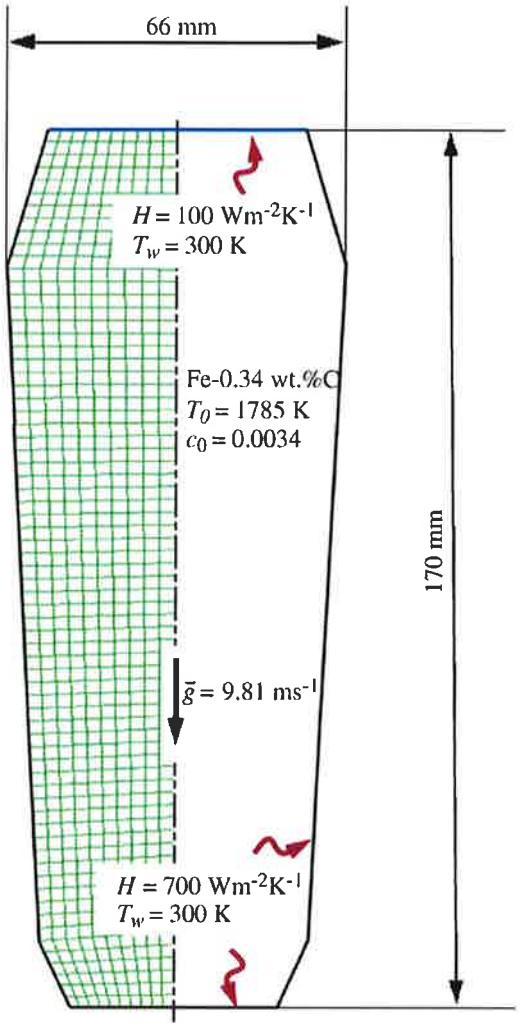

Fig. 2. Schematic of the simulated benchmark.

All other properties and parameters used for the simulation are listed in [12].

For this case the predicted macrosegregations are shown in Fig. 3:

(1) A small negative macrosegregation ($c_{mix} < c_0 = 0.34$) is found in the upper part of the surface region, specially in the upper corners where $c_{mix} < 0.33$.
(2) In the lower corners a positive macrosegregation is predicted $c_{mix} > 0.36$.
(3) A large area of positive macrosegregation with $c_{mix} > 0.38$ is located in the casting center.

In order to understand the mechanisms of the macrosegregation formation for the considered case, the solidification process together with the development of c_l and c_{mix} is shown in Fig. 4. Columnar grains start to grow from mold wall, the columnar tip front and volume fraction of columnar phase, f_c-isolines, move from the mold wall towards the bulk melt. Due to the influence of the thermal–solutal convection, the 'hot spot' moves upwards

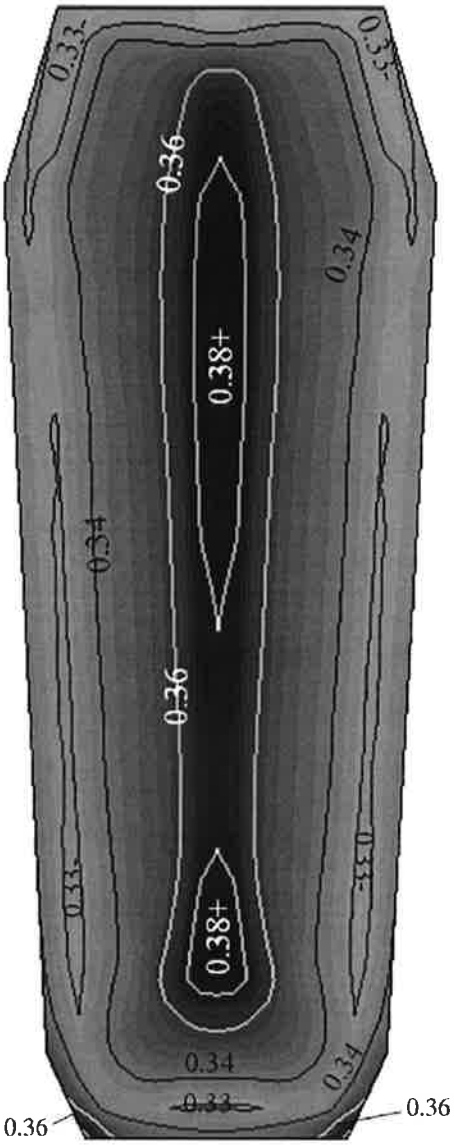

Fig. 3. Predicted macrosegregation pattern during columnar solidification in a binary (Fe–0.34 wt.% C) "steel" ingot. c_{mix} in wt.% C is shown both with isolines and gray scales: light for negative and dark for positive macrosegregations.

and is finally located above the geometrical and thermal center of the casting. During the solidification an axis symmetrical convection pattern is developed. The melt near the mold wall has a higher density due to its lower temperature ($\beta_T = 2 \times 10^{-4}\,K^{-1}$), and thus sinks downwards. The hotter melt in the center rises. One may argue that the solute-enriched interdendritic melt might partially compensate or reverse the above mentioned convection pattern. As shown in Fig. 4c, c_l near the mold wall is much higher compared to the bulk melt region. With $\beta_c = 1.1 \times 10^{-2}\,wt.\%^{-1}$, the higher the c_l, the lighter the interdendritic melt. However, it turned out that with the occurring temperature gradient, thermal buoyancy dominates against solutal buoyancy. The downwards flow in the interdendritic regions and the upwards flow in the bulk melt is the basic phenomena which leads to the formation of the final macrosegregation pattern.

Fig. 5 illustrates the macrosegregation formation mechanism in the corner regions. A local volume taken from the upper corner of the ingot is considered in Fig. 5a. The solidified columnar grains are stationary, while the interdendritic melt flows, e.g. it flows in from a vertical side of the volume and out from a horizontal. Due to solidification the interdendritic melt is segregated with solute elements, i.e. for $k < 1$ c_l is larger than the bulk melt concentration c_0. As shown in Fig. 5a, melt with $c_l^{out} > c_l^{in}$ flows out of the volume, being replaced by 'fresh' melt with nearly the bulk concentration $c_l^{in} \approx c_0$. The consequence is that the c_{mix} in the volume decreases, i.e. a negative macrosegregation occurs. In the lower bottom corners, Fig. 5b, melt with $c_l^{in} > c_0$ flows vertically into the volume. This incoming melt is enriched in solute due to segregation in the solidifying interdendritic region along the mold wall. As the solidification now takes place from that segregated melt the solid forms with a higher concentration kc_l^{in} compared to kc_0, so a positive macrosegregation forms.

The positive macrosegregations in the center (Fig. 3) are formed gradually during solidification. As shown in Fig. 4c, the interdendritic melt has always higher concentration than in the bulk melt. The interdendritic solute-enriched melt is brought out of the mush zone by the flow current, causing the c_{mix} in front of or slightly behind the columnar tip front to be enriched gradually. These positively segregated melts are not stationary, they move with the flow current, and finally meet in the casting center and form a large positive segregation zone.

3.2. Case II: macrosegregation due to grain sedimentation

Fig. 6 shows the predicted macrosegregation in the same binary "steel" ingot (Fe–0.34 wt.% C) where mixed columnar and equiaxed solidification is considered. In this case, three phases are considered: melt (indexed with l), globular equiaxed grains (e), and the stationary columnar dendrites (c). Geometry configuration and other conditions are same as for Case I (Fig. 2). The applied material properties and other modeling details are described elsewhere [12].

The predicted solidification sequence including sedimentation of the equiaxed grains, sedimentation-induced melt convection and thermal–solutal melt convection is shown in Fig. 6a and c. The presented solidification pattern agrees with the classical explanation of steel ingot solidification, which was summarized by Campbell [13]. The columnar dendrites grow from the mold wall and the columnar tip front moves inwards. The equiaxed grains nucleate near the mold walls and in the bulk melt. The columnar dendrites are stationary, whereas the equiaxed grains sink and settle in base region of the ingot. The heap of such grains in the base of the ingot has a characteristic cone-shape. Two symmetrical melt convection vortices in the ingot are induced by both thermal–solutal effects and the drag of sinking grains. The sedimentation of grains and occurring melt convection influence the macroscopic solidification sequence and thus the final phase distribution: more equiaxed grains will be found at the bottom and in the base region, and larger columnar areas in the upper part of the ingot.

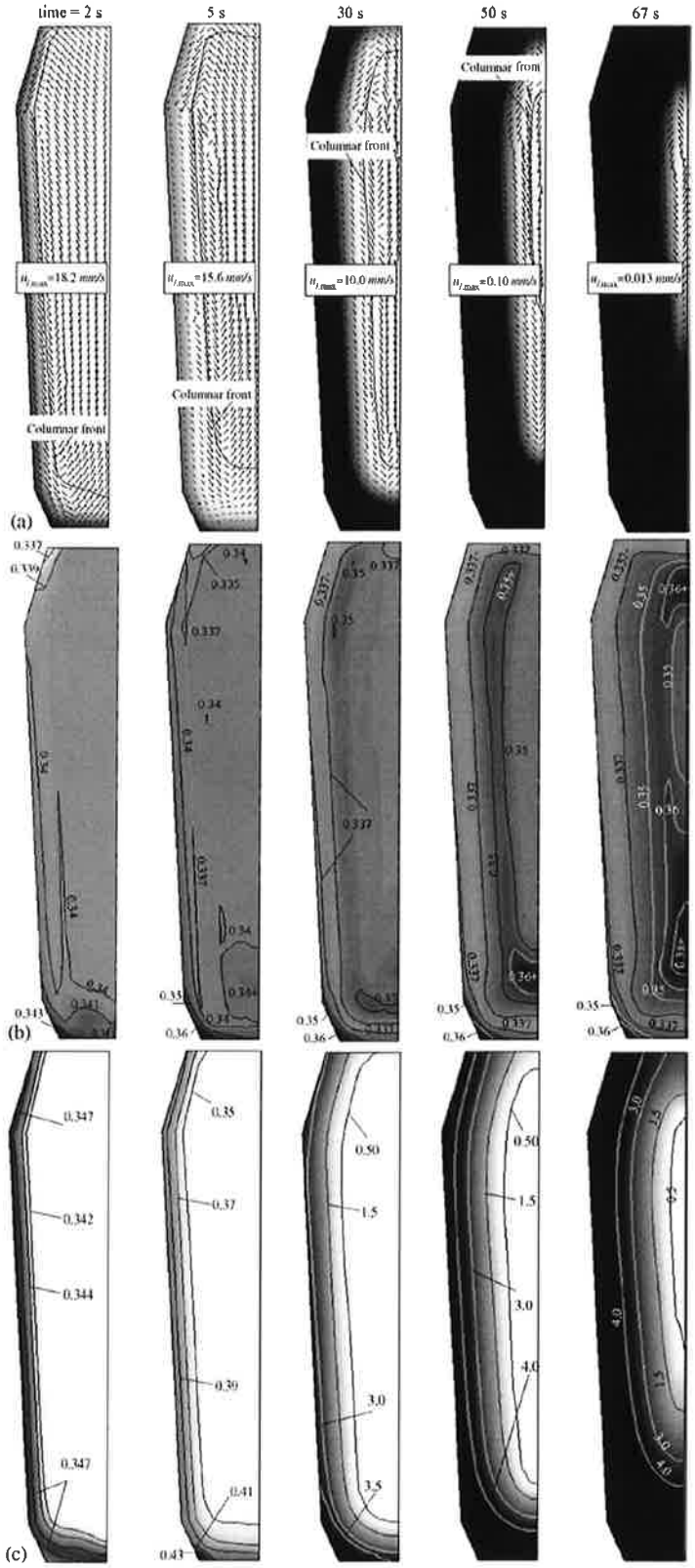

Fig. 4. Predicted solidification and macrosegregation formation in a binary "steel" ingot (Fe–0.34 wt.% C). Here only columnar solidification, but with thermal–solutal convection is considered. (a) The volume fraction of the columnar phase is shown in gray scales with light for $f_c = 0$ and dark for $f_c = 1$. The solid line shows the columnar tip front. The arrows show the velocity of melt ($\vec{u}_l$). (b) Development of macrosegregation. The mixture concentration c_{mix} is shown in both isolines and gray scales: light stands for negative and dark for positive segregations. The values at the c_{mix} isolines are in unit wt.% C. (c) Development of liquid concentration c_l again shown in both isolines and gray scales: light stands for low and dark for high concentration. The values at the c_l isolines are in unit wt.% C.

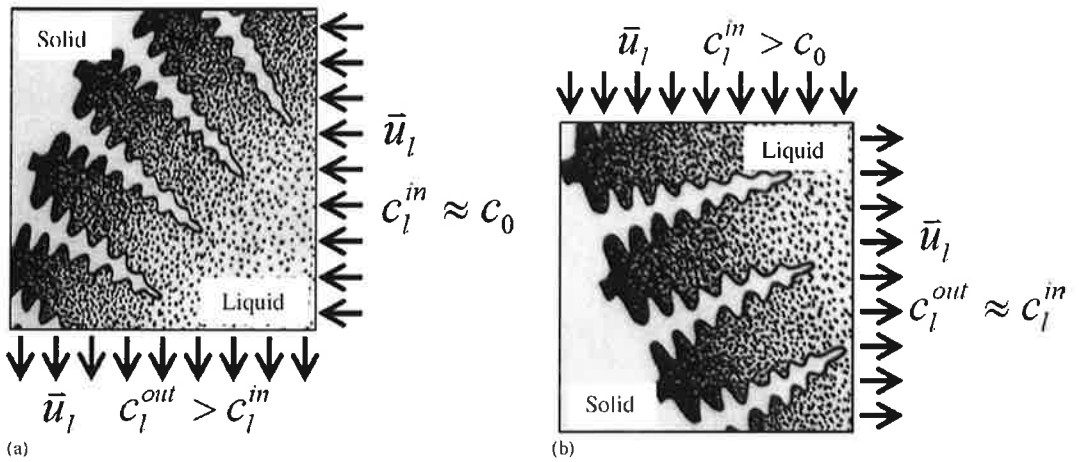

Fig. 5. Schematic illustration of negative and positive macrosegregation formation due to interdendritic flow [1]. (a) A sample volume in the upper corner. (b) A sample volume in the bottom corner.

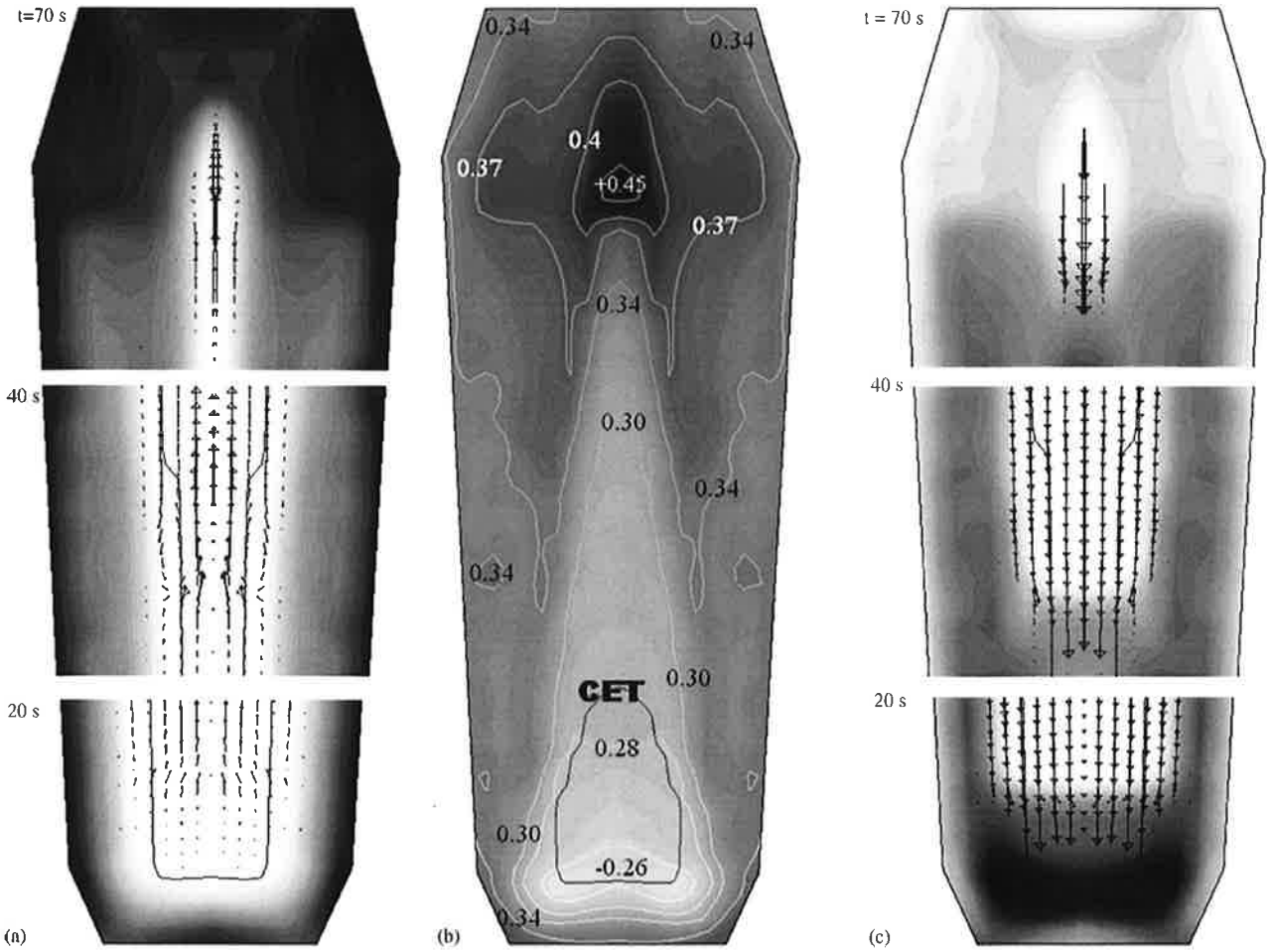

Fig. 6. Predicted solidification and macrosegregation of a binary "steel" ingot (Fe–0.34 wt.% C) in the case of mixed equiaxed and columnar solidification. c_{mix} (wt.% C) is shown with both isolines and gray scales: light for negative and dark for positive segregations. The CET is also drawn together with c_{mix} (black line). In order to illustrate the formation of macrosegregations, f_e and f_c together with $\vec{u}_l$ and $\vec{u}_e$ in three different sections (bottom, middle, top) corresponding to three different moments (20, 40, 70 s) are shown. f_c and f_e are shown with 60 gray levels from minimum (0) to maximum (0.99). The columnar tip front (solid line) overlaps the quantities f_c and f_e. (a) $f_c + \vec{u}_l$ at different time. (b) c_{mix}. (c) $f_e + \vec{u}_e$ at different time.

As the columnar tip front is explicitly tracked in the model, the simulation shows that the columnar tip fronts from both sides tends to meet in the center part of the casting. However, in the lower part of the casting the large amount of equiaxed grains stop the propagation of the columnar tip front. Its final position indicates the so-called columnar to equiaxed transition, i.e. CET. The CET separates areas where only equiaxed grains appear with those where both columnar dendrites and equiaxed grains might be found in common.

From the simulation results it becomes obvious that the main mechanism for the cone-shaped negative segregation in the base region is grain sedimentation. As the settling grains are poor in solute elements, their pile-up induces negative segregation. A further contributing factor to the strength of negative segregation arises from the flow divergence of the residual liquid through this zone at a late solidification stage. The positive segregation at the top region of the ingot is caused by the flow of the segregated melt in the bulk region (Fig. 6a). This kind of positive segregation coincides with the early experimental results of Nakagawa et al. [13,14]. Finally, it must be mentioned that channel segregations, which are frequently found in steel ingots, are not predicted with the recent model. The reason for this is that melting was not taken into account in this simulation, and that the used numerical grid is relatively coarse.

3.3. Case III: macrosegregation due to the Marangoni effect in hypermonotectic solidification

Three phases appear during solidification of a hypermonotectic alloy (Al–10 wt.% Bi): the primary liquid phase L_1, the secondary liquid phase L_2 (Bi droplets, solidification of Bi is ignored), and the solidified monotectic matrix. In practice the spatial separation of the Bi droplets from the parent melt (primary liquid phase) seems unavoidable no matter whether the alloy solidifies under normal terrestrial conditions or in a reduced gravity situation [15]. The reason for that is the Marangoni-induced droplet motion.

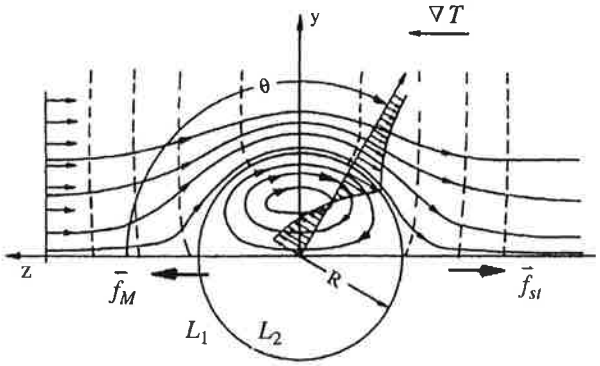

Fig. 7. Thermocapillary convection in and around the droplet. Referring to the droplet, the Marangoni force, $\vec{f}_M$, drives the droplet to move in ∇T direction. The hydrodynamic resistance called Stokes force, $\vec{f}_{st}$, points to the reverse direction as the droplet moves.

As shown in Fig. 7, when a droplet is placed in a melt with a temperature gradient, ∇T, a thermocapillary convection in/around the droplet is induced. The droplet surface is drawn from hotter towards the colder poles in order to lower the surface energy. The consequence is the motion of the droplet towards hot regions. Integration of the thermocapillary force acting on the droplet surface is defined as Marangoni force $\vec{f}_M$. As consequence, a relative velocity between droplet and matrix, $\Delta\vec{u}$, establishes, which leads to a hydrodynamic resistance, called Stokes force $\vec{f}_{st}$. Based on Stokes–Rybczynski–Hadamard approximation, Young et al. [16] have analytically deduced $\vec{f}_M$

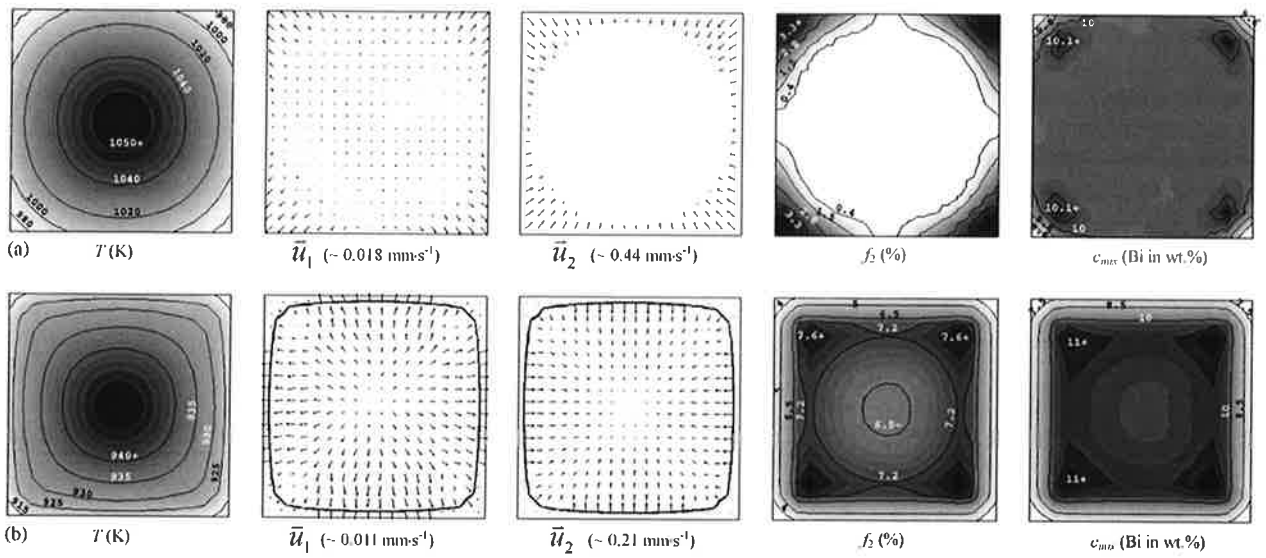

Fig. 8. Solidification sequence under 0-g condition. The arrows of the velocities are equidistantly scaled from 0 to the maximum value given, and the monotectic front (T = 925 K) is drawn together with the velocity fields. Other quantities are shown with isolines together with 30 gray levels, with dark showing the highest value and bright the lowest. (a) Time = 3.6 s. (b) Time = 15.6 s.

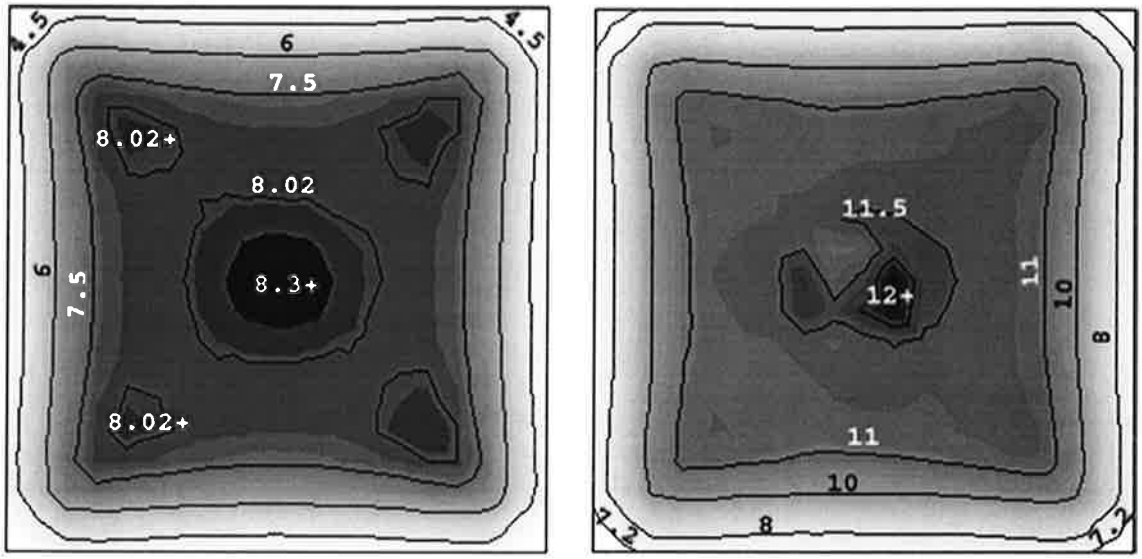

Fig. 9. The numerically predicted phase distribution and macrosegregation. All quantities are shown with isolines together with 30 gray levels, with dark showing the highest value and bright the lowest. (a) f_2 (%) and (b) c_{mix} (Bi in wt.%).

and $\vec{f}_{st}$ for a single droplet:

$$\vec{f}_M = \frac{\pi d_2^2}{(1+\mu_2/\mu_1)(2+k_2/k_1)} \frac{\partial\sigma}{\partial T} \nabla T, \tag{3}$$

$$\vec{f}_{st} = 2\pi d_2 \mu_1 \frac{1+3\mu_2/2\mu_1}{1+\mu_2/\mu_1} \Delta\vec{u}. \tag{4}$$

Here d_2 is the diameter of the Bi droplets and μ_1, μ_2, k_1 and k_2 are viscosity and thermal conductivity of the two liquids. The key parameter to model the Marangoni motion is $\partial\sigma/\partial T$, known as Marangoni coefficient, where σ is the interface energy between the two liquid phases [10,11,15].

Figs. 8 and 9 present the multiphase modeling results of a 2D square casting (90 mm × 90 mm). In the case of zero gravity (0-g) the Marangoni effect is the only mechanism for the phase separation. The mould, remaining at a constant temperature of 290 K, is assumed to be filled instantaneously with a melt of initial temperature of 1065 K. The heat exchange coefficient at the casting–mould interface is taken to be 750 W/(m^2 K). Further physical properties and modeling parameters are given in recent publications [10,11].

When the local temperature drops below the binodal point at 1062.2 K, Bi droplets start to nucleate and grow at the casting surface. The Marangoni force causes the droplets to move from the outer regions towards the casting center. The parents melt moves in reverse direction. The droplet motion results in a depletion of the secondary liquid phase in the corners and outer regions, and an enrichment of the casting center. As the casting further cools down to the monotectic point, the monotectic reaction occurs, and the droplets are entrapped in the monotectic matrix. When the solidification is finished (Fig. 9) the outer regions of the casting have a lower volume fraction of the secondary liquid phase whereas the center has a higher one. The spatial separation of the phases is the reason for macrosegregation to appear: $c_{mix} < 7.2\%$ Bi in the corners, $c_{mix} > 12\%$ Bi in the center. This tendency of phase separation agrees qualitatively with experiments performed by Walter in sounding rocket experiments with Al–Bi alloys [17].

4. Summary

The multiphase modeling results demonstrate the importance of spatial phase separation for the formation of macrosegregations.

(i) Interdendritic flow can cause both positive and negative macrosegregations. If the segregated interdendritic melt is replaced by solute lean bulk melt, negative segregation occurs. Contrariwise, positive segregation occurs.
(ii) Grain sedimentation causes negative segregation. A cone-shaped negative segregation in the base region of a 'steel' ingot is numerically predicted, which coincides with typical results observed in classical ingots.
(iii) Marangoni flow in hypermonotectic solidification may also cause macrosegregation. The presented modeling result of an Al–Bi square sample solidified under 0-g condition shows that the decomposed Bi droplets move from outer regions into the center region causing the positive macrosegregation in the center and negative in the outer surface regions. This phenomenon was also observed experimentally.

Acknowledgements

This work was partially supported by the Christian–Doppler Society (CDG), Austria, in the frame of CD Lab – *Multiphase Simulation of Metallurgical Processes*, and by the ESA-MONOPHAS project – *Advanced Bearing Alloys from Immis-*

cibles with Aluminium, for which the authors kindly acknowledge.

References

[1] M.C. Flemings, G.E. Nereo, Trans. AIME 239 (1967) 1449–1461.
[2] M.C. Flemings, R. Mehrabian, G.E. Nereo, Trans. AIME 242 (1968) 41–49.
[3] M.C. Flemings, G.E. Nereo, Trans. AIME 242 (1968) 50–55.
[4] R. Mehrabian, M. Keane, M.C. Flemings, Metall. Trans. 1 (1970) 1209–1220.
[5] C. Beckermann, Inter. Mater. Rev. 47 (2002) 243–261.
[6] A. Ludwig, M. Wu, Metall. Mater. Trans. 33A (2002) 3673–3683.
[7] M. Wu, A. Ludwig, A. Bührig-Polaczek, P.R. Sahm, Int. J. Heat Mass Transfer 46 (2003) 2819–2832.
[8] M. Wu, A. Ludwig, Adv. Eng. Mater. 5 (2003) 62–66.
[9] M. Wu, A. Ludwig, J. Luo, Mater. Sci. Forum 475–479 (2005) 2725–2730.
[10] M. Wu, A. Ludwig, L. Ratke, Mod. Sim. Mater. Sci. Eng. 11 (2003) 755–769.
[11] M. Wu, A. Ludwig, L. Ratke, Metall. Mater. Trans. 34A (2003) 3009–3019.
[12] A. Ludwig, M. Wu, Mater. Sci. Eng. A 413–414 (2005) 109–114.
[13] J. Campbell, Castings, Butterworth Heinemann Ltd, Oxford, 1991.
[14] Y. Nakagawa, A. Momose, Tetsu-to-Hagane 53 (1967) 1477–1508.
[15] L. Ratke, S. Diefenbach, Mater. Sci. Eng. 15R (1995) 263–347.
[16] N.O. Young, J.S. Goldstein, M.J. Block, J. Fluid Mech. 6 (1959) 350.
[17] H.U. Walter, Proc. RIT/ESA/SSC Workshop-ESA SP 219 (1984). ed. Järva Krog (Noordwijk, Sweden), 47–64.